Impacts of dichroic prism coatings on radiometry of the airborne imaging spectrometer APEX

Hueni, Andreas ; Schläpfer, Daniel ; Jehle, Michael ; Schaepman, Michael E

Abstract: The generation of well-calibrated radiometric measurements from imaging spectrometer data requires careful consideration of all influencing factors, as well as an instrument calibration based on a detailed sensor model. Deviations of ambient parameters (i.e., pressure, humidity, temperature) from standard laboratory conditions during airborne operations can lead to biases that should be accounted for and properly compensated by using dedicated instrument models. This study introduces a model for the airborne imaging spectrometer airborne prism experiment (APEX), describing the impact of spectral shifts as well as polarization effects on the radiometric system response due to changing ambient parameters. Key issues are related to changing properties of the dichroic coating applied to the dispersing elements within the optical path. We present a model based on discrete numerical simulations. With the improved modeling approach, we predict radiometric biases with an root mean square error (RMSE) below 1%, leading to a substantial improvement of radiometric stability and predictability of system behavior.

DOI: https://doi.org/10.1364/ao.53.005344

Impacts of dichroic prism coatings on radiometry of the airborne imaging spectrometer APEX

A. Hueni,[1,*] D. Schlaepfer,[2] M. Jehle,[1] and M. Schaepman[1]

[1]Remote Sensing Laboratories, University of Zurich, CH-8057 Zurich, Switzerland

[2]ReSe Applications, Langeggweg 3, CH-9500 Wil SG, Switzerland

*Corresponding author: ahueni@geo.uzh.ch

Received 27 February 2014; revised 20 June 2014; accepted 2 July 2014;
posted 8 July 2014 (Doc. ID 207221); published 13 August 2014

The generation of well-calibrated radiometric measurements from imaging spectrometer data requires careful consideration of all influencing factors, as well as an instrument calibration based on a detailed sensor model. Deviations of ambient parameters (i.e., pressure, humidity, temperature) from standard laboratory conditions during airborne operations can lead to biases that should be accounted for and properly compensated by using dedicated instrument models. This study introduces a model for the airborne imaging spectrometer airborne prism experiment (APEX), describing the impact of spectral shifts as well as polarization effects on the radiometric system response due to changing ambient parameters. Key issues are related to changing properties of the dichroic coating applied to the dispersing elements within the optical path. We present a model based on discrete numerical simulations. With the improved modeling approach, we predict radiometric biases with an root mean square error (RMSE) below 1%, leading to a substantial improvement of radiometric stability and predictability of system behavior.

OCIS codes: (280.0280) Remote sensing and sensors; (110.0110) Imaging systems; (300.0300) Spectroscopy; (150.1488) Calibration; (050.1930) Dichroism.

http://dx.doi.org/10.1364/AO.53.005344

1. Introduction

Airborne imaging spectrometers are used in a wide range of studies related to earth system sciences [1,2]. The generation of well-calibrated data requires an accurate instrument model based on a careful system characterization and a regular system calibration to ensure the validity of calibration coefficients over time and an instrument-specific data calibration process based on the instrument model [3], converting digital numbers (DNs) to International System of Units (SI) traceable units and essentially making data comparable over space, time, and different sensor systems [4].

Airborne imaging spectrometers are naturally prone to feature differing nominal and in-flight performances, such as changes in radiometric response or spectral band positions, commonly referred to as spectral shifts. Despite the best engineering efforts, such differences are bound to occur, brought about by air-pressure and temperature differences as well as mechanical stresses occurring during flight operations at various altitudes [5]. Such nonuniformities in imaging spectroscopy data can lead to significant distortions in both radiometrically calibrated data and derived products and need to be addressed by instrument characterization and data calibration processes [6,7]. Whether the observed nonuniformities are significant enough to warrant the employment of correction procedures will depend on the particular instrument design.

In this study we investigate the impact of spectral shifts and polarization on the radiometry of an airborne prism experiment (APEX) imaging spectrometer [8–10]. It has already been shown that APEX

1559-128X/14/245344-09$15.00/0

experiences spectral shifts during in-flight conditions, mainly brought about by changes in pressure and hence related to the operational altitude [11,12]. In the following, any constellation of environmental parameters leading to spectral misregistration will be termed a spectral shift condition.

Several years of APEX commissioning and exploitation phases have deepened the understanding of the instrument characteristics [9,13–16], particularly brought about by a stringent approach to calibration data storage, reanalysis [17], and regular vicarious validation exercises [18]. In the course of these activities, some spectral features at the start of the shortwave-infrared (SWIR) detector in the region of 950–1050 nm were noticed that could not be attributed to any target characteristic nor to any known atmospheric feature or absorption of solidified gases, as might happen due to condensation under low temperatures on optical surfaces. An example of the most notable of these artifacts at 1026 nm appearing in a SWIR spectrum acquired over a vegetation target at a flight altitude of 5000 m above sea level and calibrated in the APEX processing and archiving facility [19] is given in Fig. 1.

The APEX design involves the use of a dichroic coating (DIC) applied on the SWIR prism, acting as a beam splitter between the visible/near-infrared (VNIR) (376–1004 nm) and SWIR channels (901–2505 nm) with a spectral overlap of 103 nm between channels. The DIC exhibits significant spectral features, giving rise to a hypothesis of radiometric impacts of the coating under spectral shift conditions. In this contribution, we further develop the APEX calibration model to include characterization and compensation of DIC induced effects based on polarization and spectral shift analysis.

2. Material and Methods

The following subsections will detail the nominal characteristics of the APEX sensor and the laboratory characterizations required to enable the building of a model that can simulate the impact of spectral shifts on radiometry.

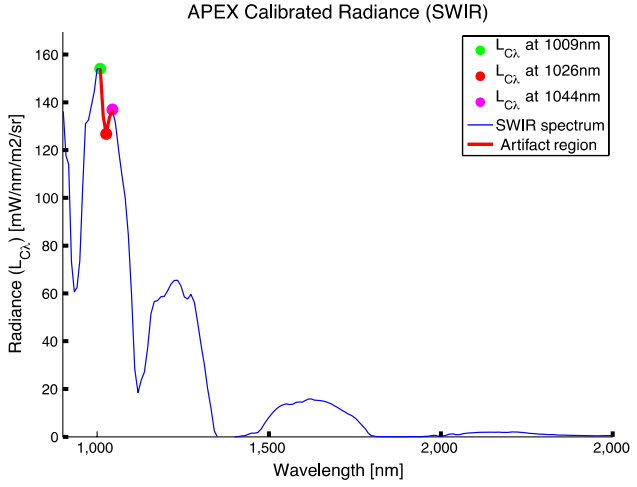

Fig. 1. APEX calibrated SWIR radiance spectrum showing an unexpected absorption feature at 1026 nm where a smooth transition between 1009 and 1044 nm is expected.

A. APEX

APEX is a push-broom system, relying on prisms to disperse the incoming light. Two separate detectors are used to image the VNIR and the SWIR part of the spectrum with a spectral overlap between the two channels. The splitting of incoming light into the two channels is accomplished by means of a DIC applied to the second surface of the SWIR prism (Fig. 2). Ideally, such a coating would be a perfect bandpass with a dirac transition from zero to 100% transmission at the splitting wavelength. In practice, such coatings feature neither a clean step nor are their transmissions a linear transition between zero and one over their spectral range. The coating used in APEX was procured by Swiss Optic (www.swiss-optic-lenses.com) and its nominal transmission as specified by industry is not only spectrally but also polarization dependent (Fig. 3).

Essentially, the incoming radiance signal is modulated by the DIC transmission. Radiometric calibration of the system inherently compensates for the DIC transmission as DNs are related to at-sensor radiances through a first-order polynomial, i.e., the radiometric coefficients of each spatiospectral pixel compensate for the impact of the DIC transmission. At this point, the recorded DNs represent the spectrally convolved, DIC-modified signal. However, under spectral shift conditions, the features of the DIC are shifted relative to the detector and appear therefore shifted by fractions of pixels. Consequently, the radiometric coefficients no longer properly compensate for the DIC transmission.

A modeling of these dependencies requires an instrument model that describes the spectral characteristics of the optical path and the detailed function of the spectral shift.

B. Spectral Shift Characteristics

Spectral shifts of APEX have previously been analyzed based on spectral features of both the internal

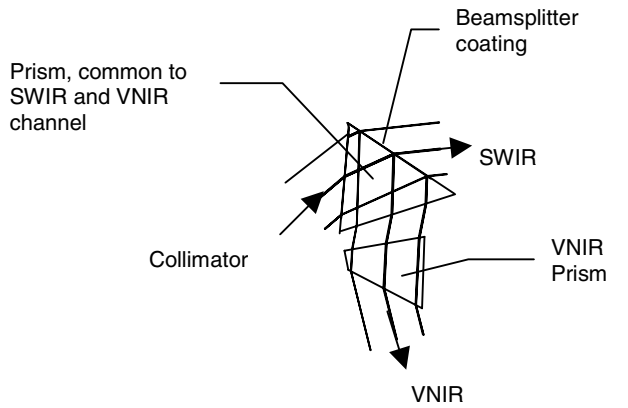

Fig. 2. Prisms and channel splitting in the APEX optical subunit [20].

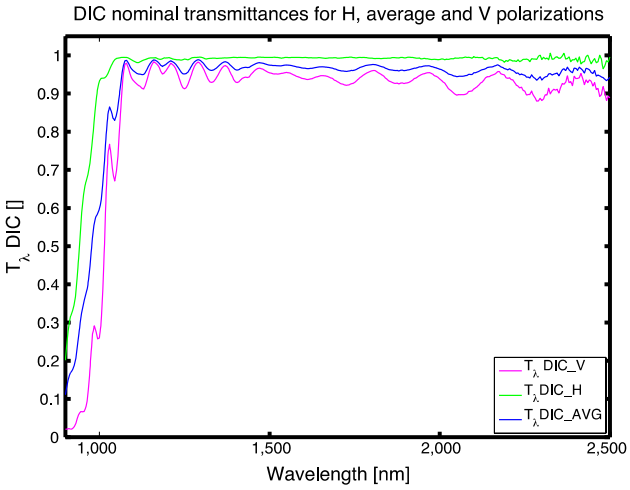

Fig. 3. Nominal DIC transmittances for H, V, and average polarizations.

in-flight calibration facility and the atmosphere during imaging runs [12]. However, these methods can only provide shift estimates at selected spectral bands where absorption features occur. For the study at hand, shift characteristics must be known on a band-per-band basis. Such data can only be acquired under laboratory conditions where a wavelength-specific system input can be provided by a monochromator. The goal of the shift characteristics experiment carried out at the APEX calibration home base (CHB) [21] was to establish changes to the spectral response functions (SRFs) via the determination of center wavelengths (CWs) and full width at half-maximum (FWHM) under controlled spectral shift conditions applying a full spectral characterization, i.e., sampling all spectral bands. The standard spectral calibration applies a spatiospectral sampling pattern in order to accomplish these measurements in a reasonable time [17]. In the case of the shift experiment, a contiguous spectral sampling was applied to the nadir pixel only as a full spatial and spectral characterization would be too time consuming. The off-nadir spatial positions are expected to have the same characteristics in terms of spectral shift response, only modified by the specific wavelength center smile (spectral misregistration).

Variations in spectral shift were achieved by setting the absolute internal pressure of the system by means of the pressure regulation unit (PRU). By default, the PRU maintains a nominal 200 mbar overpressure of the optical subunit (OSU) in relation to the ambient pressure, drawing on a pressure bottle to supply the N_2 atmosphere within the OSU. For the shift experiment, the PRU was operated manually, providing nominal delta pressure steps of 50 mbar ranging between ambient pressure and 200 mbar overpressure. The resulting spectral shift is the product of the change in N_2 medium density leading to a change of the gaseous refractive index and thus to a change in the prism refraction and the observed dispersion, not withstanding impacts of the pressure on mechanical deformation. The difference between CWs and FWHMs acquired under these different pressure conditions leads to functions describing the per band change in CW and FWHM, required by the DIC modeling.

The absolute OSU pressure range of 900–1100 mbar tested in the laboratory is different from the typical pressures ranges encountered during in-flight conditions where a minimal system pressure of 550 mbar is reached for the maximal operational altitude of 7500 m above sea level obtainable with the Dornier DO-228 standard APEX carrier. However, as the spectral shift is assumed to be a function of the N_2 density only and the refractive index of N_2 is a linear function of pressure [22], it is expected that the shift response of the system can be reliably extrapolated to the pressures encountered in-flight.

C. Optoelectronic System Model

Preliminary results led to the conclusion that the nominal DIC transmission supplied by industry did not fully describe the attenuation of the signal in the optoelectronic path. Indicative of this was that the shift simulation fell short of simulating the actual impact of shifts on the recorded digital numbers (DN_λ). This led to the assumption that further components of the optoelectronic system do have spectrally dependent behaviors. For a realistic simulation of the effect of shifts on radiometry, all optoelectronic components that change their behavior under shift conditions must be accounted for.

Generally, the optical path plus electronics including amplifiers and digitizers can be described by [23–25]

$$L_{S\lambda} \cdot T_\lambda \cdot \mathrm{QE}_\lambda \cdot a_\lambda + b_\lambda = \mathrm{DN}_\lambda, \tag{1}$$

where:

$L_{S\lambda}$ = at-sensor radiance

T_λ = transmittance of the optical chain

QE_λ = quantum efficiency

a_λ = amplifier gain

b_λ = amplifier offset.

In practice, the radiometric calibration of the system is reduced to gain and offset coefficients obtained by fitting first-order polynomials to laboratory-generated at-sensor radiances and measured system responses in DN for several radiance levels:

$$L_{S\lambda} = \mathrm{DN}_\lambda \cdot g_\lambda + o_\lambda \tag{2}$$

where:

g_λ = radiometric gain

o_λ = radiometric offset.

The radiometric offset should ideally be zero if the DNs have been corrected for the dark current signal

and any nonlinearities with the gain g_λ encapsulating T_λ, QE_λ and amplifier gain a_λ. It is thus valid to use the inverse gain g_λ as combined system transmittance $T_{C\lambda}$.

D. Sensitivity Assessment of Spectral Shifts

The radiometric error caused by spectral shifts can be quantified by a numerical modeling approach simulating a range of spectral shifts from a zero shift to the maximum spectral shift observed under in-flight conditions.

Figure 4 illustrates the data flow of the simulation. The whole simulation is part of the APEX calibration information system (CAL IS) [17] and can therefore easily access system characteristics data stored in the CAL IS database. The model is parameterized by (a) the overall system transmission $T_{C\lambda}$ of a selected polarization angle, (b) nominal CWs and FWHMs, (c) shift change vectors for CWs and FWHMs, and (d) shift simulation range and resolution. The CWs and FWHM change vectors are determined based on data acquired during the spectral shift sampling experiment. These vectors are based on differences between estimated SRF parameters and require some smoothing due to oscillations of the monochromator output wavelengths. The smoothed vectors are then used to generate spectral shift realizations at a defined simulation step size, set to 0.1 nm and ranging from +25 to −25 nm to ensure that any possible shift occurring under in-flight conditions is covered, i.e., the maximum being equivalent to a spectral shift of 2.5 pixels for the SWIR band with the highest FWHM. Shift values between zero shift and maximum shift are calculated using a first-order function. This linear behavior has been ascertained within the laboratory-based shift experiment.

The processing steps detailed below are carried out for all parameters in the CWs and FWHM shift realization table, leading to calibrated radiances for all shift realizations. The at-sensor radiance variable to be run through the model is by default a quartz tungsten halogen (QTH) lamp radiance selected from the CAL IS database but can essentially be any input radiance if so required. The input radiance is attenuated by the combined transmission $T_{C\lambda}$ for a specified polarization angle. As $T_{C\lambda}$ is essentially the inverted system gain, the signal is converted to DNs at this point. The DN spectrum is subsequently convolved to APEX, parameterized with nominal CWs and FWHMs modified with the spectral shift realization data. The result is a DN spectrum sampled by a spectrally shifted APEX sensor. The DNs are then calibrated to radiances by applying APEX gains and offsets. These radiometric coefficients are acquired in the laboratory under 200 mbar nominal overpressure, i.e., they represent the CHB calibration where no shift is present. In this manner, the radiometric calibration applies coefficients that compensate the attenuation of the signal by optical path transmission features but only so in the unshifted case, i.e., replicating the effect of the actual APEX radiometric calibration, where CHB coefficients are applied to DNs stemming from a shifted spectrum.

E. Polarization Characteristics

The impact of polarization on the recorded signal due to the polarization-dependent DIC transmission had

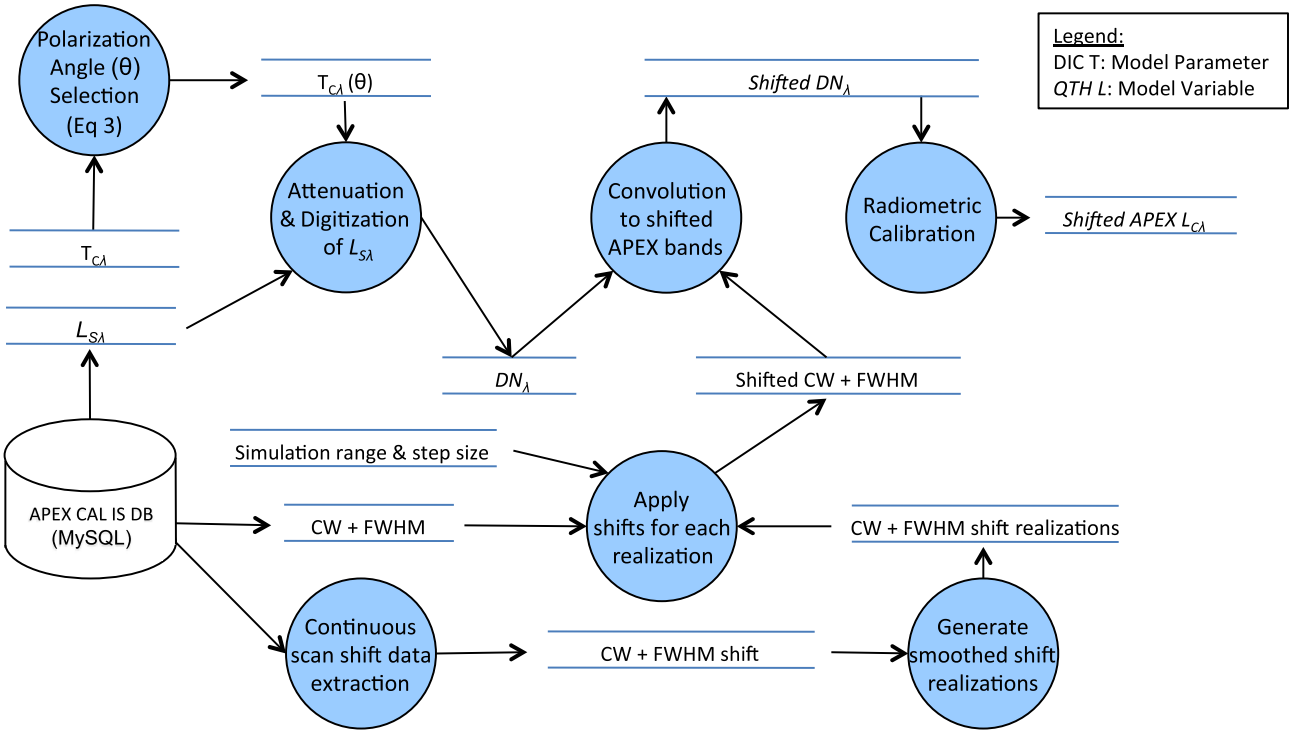

Fig. 4. Data-flow diagram of the DIC model.

up to this point been a theoretical notion, contrary to the impact of a shifted DIC transmission, which could be observed in imaged data in an obvious way, the reason being that polarization remains a poorly studied subject in spectroscopy and remains unaccounted for in most application studies. Consequently, no bias relatable to polarization had been identified. To confirm the existence of a polarization dependency of the recorded signal, a test was run in the CHB by mounting a polarization filter on a stepping-motor-driven mount and placing it between integrating sphere port and APEX baffle. Angles set on the mount ranged from 0° to 180° in 15° steps. These CHB-based polarization measurements were subjected to a Fourier analysis, yielding the offset between external and internal polarization angles, as well as the minimum, mean, and maximum transmittance values for V, average, and H polarizations. These transmittances were then normalized to the average transmittance.

F. Sensitivity Assessment of Polarization

Polarization received at the sensor may occur independently of any spectral shifts of the instrument and is governed by the target, the atmosphere, and the observational geometry. In order to build a model that can estimate the changes in signal and may later be used to correct in-flight data, a combined model for polarization and spectral shifts must be built that can predict the resulting DN for a given polarization and a particular spectral shift.

In practice, a shift simulation is carried out for each polarization-dependent system transmission, described by the normalized transmittance $T_{C\lambda-\mathrm{norm}}(\theta)$ (Fig. 5). The simulation is parameterized by a polarization-dependent system transmittance $T_{C\lambda}(\theta)$, calculated from the normalized H polarization transmittance and the average polarization transmittance:

$$T_{C\lambda}(\theta) = T_{C\lambda}(45) + (T_{C\lambda\text{-}H\text{-norm}} - T_{C\lambda}(45)) \cdot \cos(2\theta), \tag{3}$$

where

$$T_{C\lambda}(45) = \text{system transmittance at average polarization}$$
$$T_{C\lambda\text{-}H\text{-norm}} = \text{normalized system transmittance at } H \text{ polarization}$$
$$\theta = \text{polarization angle.}$$

The numerical simulation of polarization was carried out between 0° and 90° with a step size of 1° and in combination with the shift simulation at 0.1 nm intervals resulting in a total of 45,500 realizations.

3. Results

This section introduces some of the intermediate data used to build the numerical model. The results of the model are documented and compared to laboratory measurements.

A. Polarization Characteristics

The result of the CHB-based polarization experiment was two-fold: (a) recorded APEX signals are polarization dependent and the system response versus polarization angle is sinusoidal with the minima/maxima appearing at V and H polarizations, respectively (Fig. 6), and (b) the differences in transmittance between V and H to the average, i.e., the 45° polarization, are larger than the nominal values supplied by industry, as is illustrated by comparing the nominal to the estimated transmittance normalized to the average transmittance (Fig. 5). The large variation in the first few bands of the transmittance spectra is most prominent and highlights the spectral region most sensible to polarization.

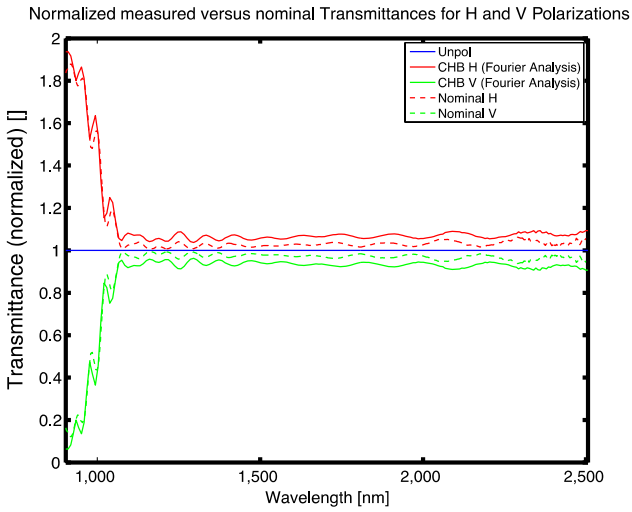

Fig. 5. Normalized nominal and Fourier analysis extracted transmittances for H and V polarizations.

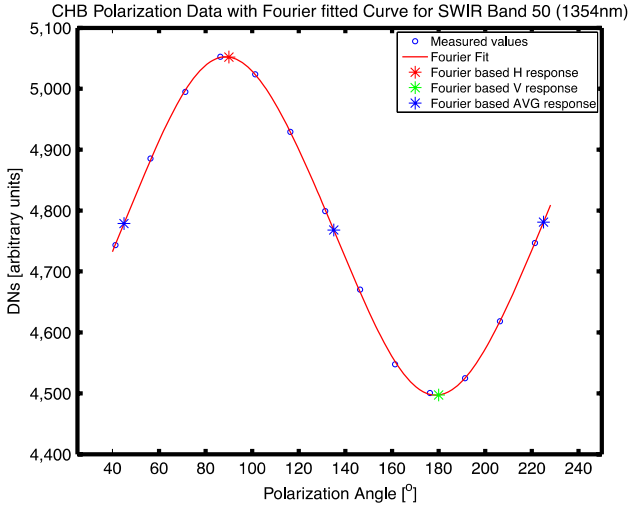

Fig. 6. Measured system response with changing polarization angle for SWIR band 50 (1354 nm) and fitted Fourier analysis-based curve with estimated values for H, V, and average polarizations.

It is however obvious that a transmittance estimation based on CHB measurements can only provide an approximation of the true transmittance, first through biases of angular nature in the measurement setup and second due to the spectral convolution by the instrument, which necessarily degrades the retrieved transmittance spectrum.

B. Center Wavelengths and FWHM Realizations

This section presents some of the intermediate data that are used to drive the discrete numerical simulation, namely the CHB-based nominal CWs and FWHM vectors and the CW and FWHM change matrices.

The nominal CWs and FWHMs represent the APEX SRFs at nadir position acquired under zero-shift conditions at the CHB (Fig. 7).

The CW change matrix contains the deviations in nanometers from the nominal, i.e., zero shift instrument state for each spectral band. The FWHMs change matrix holds similar information for the bandwidth per band. Both matrices contain N realizations, where N is given by the simulation range and the chosen step size (Fig. 8).

C. Impact of Spectral Shifts on Radiometry

Given the large number of realizations resulting from the iterations over polarization angles and spectral shifts, only some selected results can be shown here. The impact of spectral shifts on the radiometry is illustrated for the unpolarized state of at-sensor radiance. The variation in DN brought about by the shifted, DIC-modified input signals results in a maximum difference of the shifted realizations to the nominal of 102% at 919 nm (Fig. 9).

The first bands of the SWIR are most heavily influenced due to the high gradient of the DIC in that spectral region. Other regions of high difference are located next to rapid changes in DN gradients, e.g., at atmospheric absorption features such as the H_2O feature at 1370 nm.

The variation of radiances for these shift realizations demonstrates the significant impact of spectral

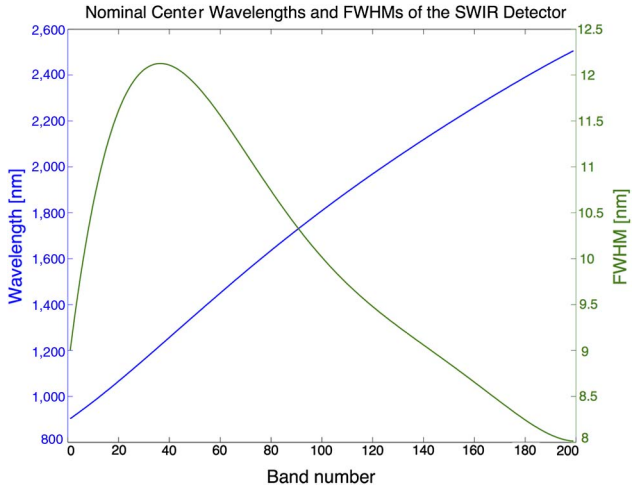

Fig. 7. Nominal CWs and FWHMs of the SWIR detector.

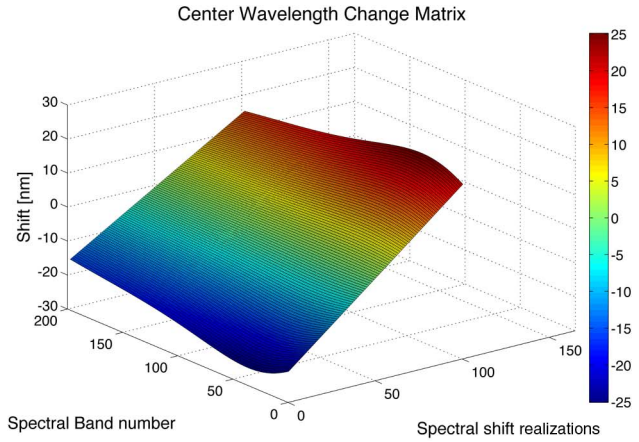

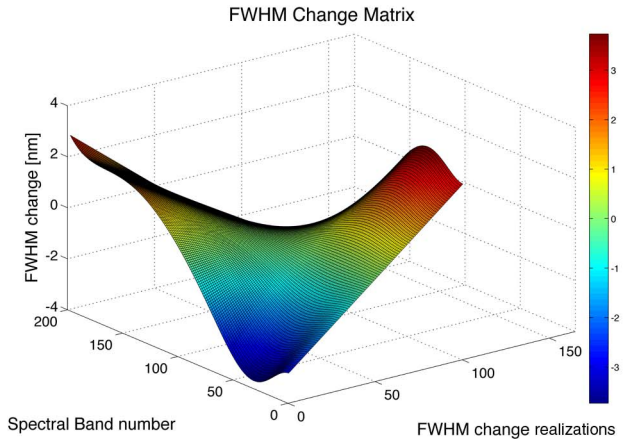

Fig. 8. CW and FWHM change matrices (visualized with a simulation step size of 0.5 nm).

shifts on radiometry (Fig. 10). The fanning out of radiances toward the lower bands of the SWIR may appear like an aggravation, but the relative differences to the unbiased at-sensor radiance are the same as for the DN realizations to the zero-shift

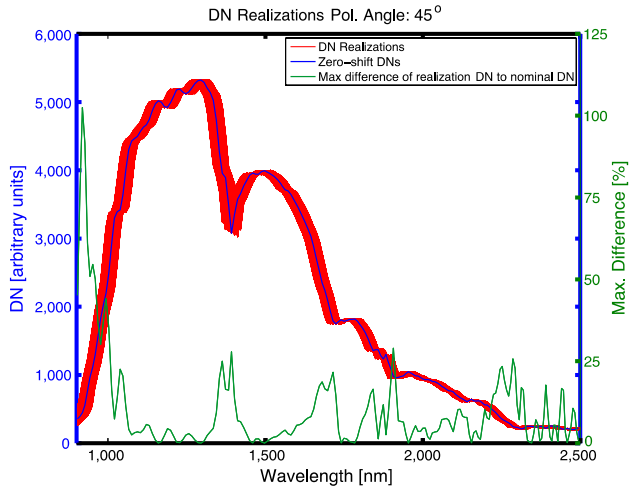

Fig. 9. DN realizations compared to the zero-shift DN for spectral shifts up to ±2.5 pixels and according maximum relative differences between nominal and realization DNs.

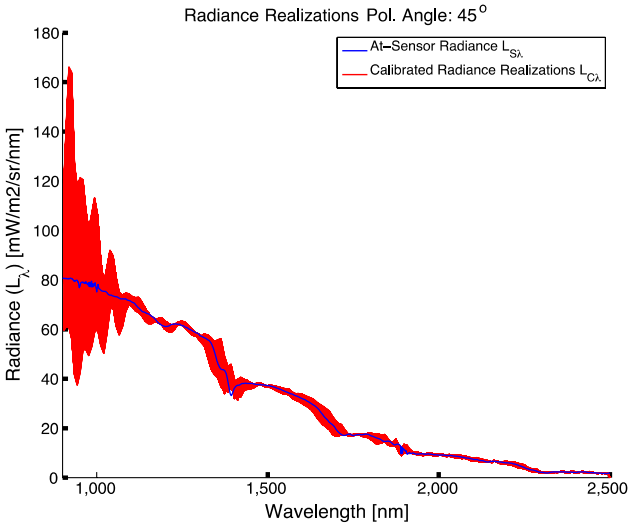

Fig. 10. Comparison of at-sensor radiance $L_{S\lambda}$ with calibrated radiance realizations $L_{C\lambda}$ for uncorrected spectral shifts up to ± 2.5 pixels.

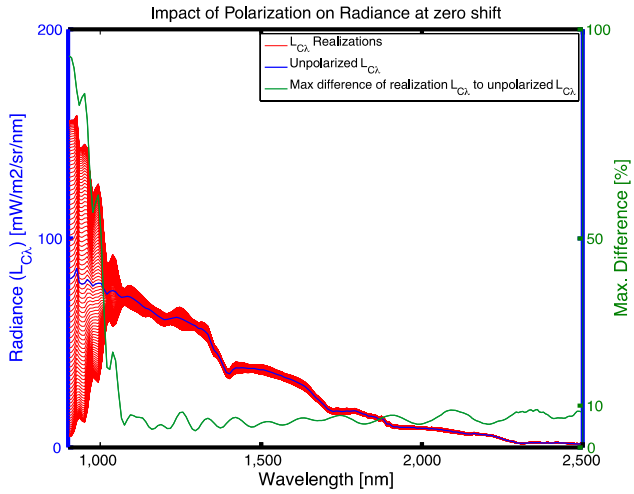

Fig. 11. Impact of polarization on radiances at zero spectral shift and maximum relative differences between at-sensor and realization radiances.

DNs. The reason for this wide spread lies in the comparatively high gains that compensate for the low signal due to the low transmission of the DIC in the transition zone from reflecting to transmitting behavior.

D. Impact of Polarization on Radiometry

In order to study the effect of polarization independently of any impact of spectral shifts, the simulation results for a zero-spectral shift are presented hereafter.

Polarization angles ranging from 0° to 90° create an envelope around the unpolarized DN signature. Similar to the effect of spectral shifts on radiometry, applying the radiometric calibration creates a large spread of radiances in the first bands of the SWIR (Fig. 11). Maximum relative differences to the unpolarized state reach 94%, dropping down to a level of around 7% after 1066 nm. Note that this variation is the maximum variation under the assumption of a fully polarized signal.

E. Constant Albedo Example under Simulated In-Flight Conditions

The above two sections illustrated the impact of spectral shifts and polarizations on the radiometry in an isolated manner for the case of a QTH input spectrum, as may be observed under laboratory conditions. In the following, we consider an at-sensor radiance spectrum of a 0.2 albedo surface under a typical spectral shift condition appearing during in-flight conditions and assuming a medium degree of polarization of 5%. This test case is based on calculations by [26], who carried out a theoretical assessment of the polarization effects expected for APEX.

To obtain a realistic at-sensor radiance spectrum, an artificial target signature with an albedo of 0.2 for all wavelengths between 350 and 2500 nm was fed into a Modtran [27] simulation using the Modo interface [28]. The simulation computed a radiance spectrum at 3000 m above sea level with a sun zenith angle of 30°, assuming a mid-latitude summer atmosphere and a visibility of 23 km. The parameterization of Modtran *per se* is, however, of little importance on the error estimation as the DIC model is linear. The goal of this Modtran run was to feed the DIC simulation with a spectrum that exhibits the high spectral gradients typically appearing at the edges of atmospheric absorption bands.

The simulated radiance spectrum was fed into the DIC model, in effect substituting the QTH lamp radiance. The degree of polarization of 5% was converted to a polarization angle of 42.75° as the model was built for parameterization by polarization angles and not degrees of polarization. The resulting model output could then be queried to show the isolated as well as combined effects of spectral shift and polarization on the DN and calibrated radiance spectra (Fig. 12).

The polarization alone leads to differences of up to a maximum of 10% at 960 nm. The spectral shift results in massive relative differences, mainly brought about by the high gradients in the spectrum next to absorption features as well as by near-zero values within absorption features.

F. Comparison of Simulated and Measured Data

This section evaluates the APEX DIC model in terms of its ability to replicate shifted laboratory measurement results acquired at 200 and 0 mbar delta pressure between OSU and ambient pressures on an integrating sphere made radiometrically traceable to the German national standard via the RASTA device [29,30]. Model realizations were selected based on the expected shift for the given absolute pressure. The comparisons were carried out on radiance levels. Both CHB DNs and simulated DNs were calibrated to radiances within the APEX CAL IS

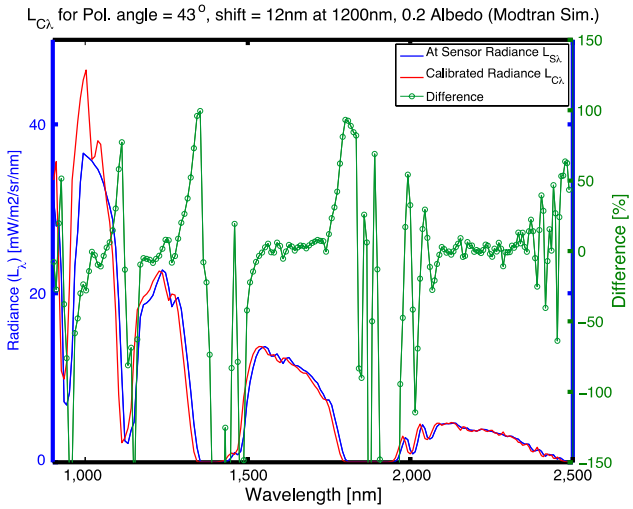

Fig. 12. At-sensor radiance and calibrated radiance spectrum of a 0.2 albedo target showing the combined effects of spectral shift and polarization and the according difference spectrum in percent.

using radiometric calibration coefficients derived from CHB measurements. Simulated and measured shifted spectra are virtually identical (Fig. 13).

The difference spectrum of simulated and measured spectra for the shifted case shows higher errors at the water vapor absorption bands as well as toward the end of the SWIR where the signal is rather low. A pattern with differences up to 4.8% remains between 900 and 1200 nm, directly related to spectral features caused by the DIC. It must therefore be concluded that the actual DIC transmission variation exceeds the nominal. The simulation parameterized with a total system transmittance estimated from the radiometric gain can estimate the true effect of spectral shifts on the radiometry with an overall RMSE below 0.8%.

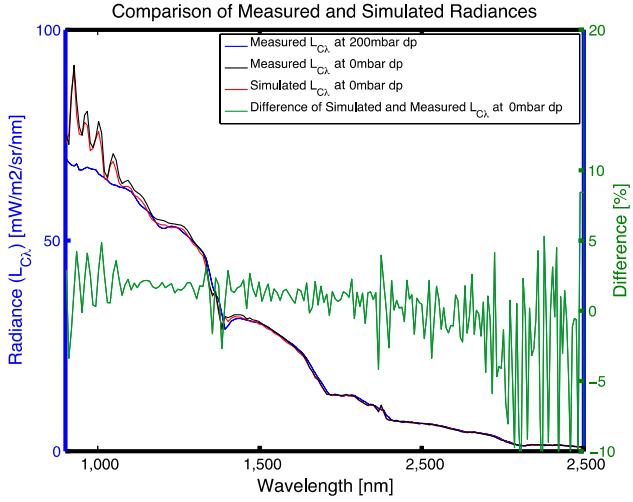

Fig. 13. Comparison of measured and simulated integrating sphere radiances under spectral shift conditions of 200 mbar delta pressure.

4. Discussion

This study investigated the effects of spectral shifts and polarization on radiometry in combination with a DIC used for beam splitting between APEX VNIR and SWIR channels. The results highlight on one hand the large effects such a coating can have on the recorded spectra and, on the other hand, the well-known high impact of uncorrected spectral shifts on radiometry [31]. As a consequence, two corrections must be implemented to compensate these effects: (a) a DIC specific correction, based on the model developed in this study, and (b) a spectral shift correction by either resampling or by supplying the estimated CWs along with the calibrated dataset.

The correction of polarization effects could potentially make use of the VNIR and SWIR channel overlap as suggested by [26]. This approach requires, however, a compensation of spectral shift-induced effects first for both instrument channels and a reliable radiometric calibration in the overlap where it is generally hampered by low signals due to reduced VNIR quantum efficiency and low DIC transmission.

While the effects described in this work are APEX-specific due to its particular response to pressure-induced spectral shifts and its specific optical setup, including a DIC, one may expect to find similar effects in other sensor systems whenever the optical path comprises components with gradients in their transmissions that would lead to significant modulation of the light reaching the detector under spectral shift conditions.

5. Conclusions

Numerical simulations of the impact of spectral shifts and polarized at-sensor radiances in combination with the DIC acting as a beam splitter have clearly demonstrated the large impact these two parameters can have on the radiometry of the APEX SWIR detector. In particular, the bands where the coating displays a high gradient of transmission are prone to be biased with as much as 102% error for a maximum simulated shift of 2.5 pixels.

The simulation can reproduce laboratory-based shift measurements with an RMSE below 0.8% with larger errors appearing in the regions of high coating transmission gradients.

Future work will concentrate on the refinement of the optical transmission parameterization and on creating a DIC model for the APEX VNIR channel. Furthermore, algorithms will have to be developed that use the derived model to correct image data for the effects of spectral shifts and, potentially, polarization.

This research was carried out within the EURAMET EMRP ENV-04 project. The EMRP is jointly funded by the EMRP participating countries within EURAMET and the European Union.

References

1. M. E. Schaepman, S. L. Ustin, A. J. Plaza, T. H. Painter, J. Verrelst, and S. Liang, “Earth system science related imaging

spectroscopy—An assessment," Remote Sens. Environ. **113**, S123–S137 (2009).
2. National Research Council, *Earth Science and Applications from Space: National Imperatives for the Next Decade and Beyond*, S. S. Board, ed. (The National Academies, 2007), p. 456.
3. D. Schläpfer, A. Boerner, S. Bojinski, and M. Schaepman, "Calibration concept for the airborne PRISM experiment (APEX)," Can. J. Remote Sens. **26**, 455–465 (2000).
4. M. Dinguirard and P. N. Slater, "Calibration of space-multispectral imaging sensors: a review," Remote Sens. Environ. **68**, 194–205 (1999).
5. B.-C. Gao, M. J. Montes, and C. O. Davis, "Refinement of wavelength calibrations of hyperspectral imaging data using a spectrum-matching technique," Remote Sens. Environ. **90**, 424–433 (2004).
6. J. Nieke, D. Schläpfer, F. Dell'Endice, J. Brazile, and K. I. Itten, "Uniformity of imaging spectrometry data products," IEEE Trans. Geosci. Remote Sens. **46**, 3326–3336 (2008).
7. D. Schläpfer, J. Nieke, and K. Itten, "Spatial PSF nonuniformity effects in airborne pushbroom imaging spectrometry data," IEEE Trans. Geosci. Remote Sens. **45**, 458–468 (2007).
8. K. Itten, F. Dell'Endice, A. Hueni, M. Kneubühler, D. Schläpfer, D. Odermatt, F. Seidel, S. Huber, J. Schopfer, T. Kellenberger, Y. Bühler, P. D'Odorico, J. Nieke, E. Alberti, and K. Meuleman, "APEX—The hyperspectral ESA airborne prism experiment," Sensors **8**, 6235–6259 (2008).
9. M. Jehle, A. Hueni, A. Damm, P. D'Odorico, J. Weyermann, M. Kneubühler, D. Schläpfer, M. Schaepman, and K. Meuleman, "APEX—Current status, performance and validation concept," in *IEEE Sensors* (IEEE, 2010), pp. 533–537.
10. M. Schaepman, M. Jehle, A. Hueni, P. D'Odorico, A. Damm, J. Weyermann, F. D. Schneider, V. Laurent, C. Popp, F. C. Seidel, K. Lenhard, P. Gege, C. Küchler, J. Brazile, P. Kohler, L. D. Vos, K. Meuleman, R. Meynart, D. Schläpfer, and K. I. Itten, "Advanced radiometry measurements and Earth science applications with the airborne prism experiment (APEX)," Remote Sens. Environ, submitted.
11. P. D'Odorico, E. Alberti, and M. Schaepman, "In-flight spectral performance monitoring of APEX," Appl. Opt. **49**, 3082–3091 (2010).
12. P. D'Odorico, L. Guanter, M. E. Schaepman, and D. Schläpfer, "Performance assessment of onboard and scene-based methods for airborne prism experiment spectral characterization," Appl. Opt. **50**, 4755–4764 (2011).
13. K. Itten, K. Meuleman, M. Schaepman, E. Alberti, B. Bomans, F. Dell'Endice, P. D'Odorico, A. Hueni, J. Nieke, D. Schläpfer, and G. Ulbrich, "First test results of the airborne dispersive pushbroom imaging spectrometer APEX," in *EARSeL SIG IS* (EARSeL, 2009), p. 6.
14. A. Hueni, S. Sterckx, M. Jehle, P. D'Odorico, K. Vreys, B. Bomans, J. Biesemans, K. Meuleman, and M. Schaepman, "Operational status of APEX and characteristics of the APEX open science data set," in *IGARSS* (IEEE, 2012), pp. 5009–5012.
15. A. Hueni, S. Sterckx, and M. Jehle, "Operational calibration of APEX," in *IGARSS* (IEEE, 2013), pp. 4423–4426.
16. M. Jehle, A. Hueni, K. Lenhard, A. Baumgartner, and M. E. Schaepman, "Detection and correction of radiance variations during spectral calibration in APEX," IEEE Lett, submitted.
17. A. Hueni, K. Lenhard, A. Baumgartner, and M. Schaepman, "The APEX (airborne prism experiment—imaging spectrometer) calibration information system," IEEE Trans. Geosci. Remote Sens. **51**, 5169–5180 (2013).
18. A. Hueni, M. Jehle, A. Damm, A. Burkart, and M. Schaepman, "Spectroscopy information systems for earth system science," in *ESA PV2013 Workshop* (ESA, 2013), pp. 220–230.
19. A. Hueni, J. Biesemans, K. Meuleman, F. Dell'Endice, D. Schläpfer, S. Adriaensen, S. Kempenaers, D. Odermatt, M. Kneubuehler, J. Nieke, and K. Itten, "Structure, components and interfaces of the airborne prism experiment (APEX) processing and archiving facility," IEEE Trans. Geosci. Remote Sens. **47**, 29–43 (2009).
20. OIP Sensor Systems, APEX OSU Optical Design Description (2005).
21. P. Gege, J. Fries, P. Haschberger, P. Schötz, H. Schwarzer, P. Strobl, B. Suhr, G. Ulbrich, and W. J. Vreeling, "Calibration facility for airborne imaging spectrometers," ISPRS J. Photogramm. Remote Sens. **64**, 387–397 (2009).
22. G. Z. Xiao, A. Adnet, Z. Zhang, F. G. Sun, and C. P. Grover, "Monitoring changes in the refractive index of gases by means of a fiber optic Fabry–Perot interferometer sensor," Sens. Actuators A **118**, 177–182 (2005).
23. A. Börner, L. Wiest, R. Reulke, R. Richter, P. Keller, M. Schaepman, and D. Schläpfer, "SENSOR: a tool for the simulation of hyperspectral remote sensing systems," ISPRS J. Photogramm. Remote Sens. **55**, 299–312 (2001).
24. J. Nieke, M. Solbrig, and A. Neumann, "Noise contributions for imaging spectrometers," Appl. Opt. **38**, 5191–5194 (1999).
25. G. Lichtenberg, Q. Kleipool, J. M. Krijger, G. van Soest, R. van Hees, L. G. Tilstra, J. R. Acarreta, I. Aben, B. Ahlers, H. Bovensmann, K. Chance, A. M. S. Gloudemans, R. W. M. Hoogeveen, R. Jongma, S. Noël, A. Piters, H. Schrijver, C. Schrijvers, C. E. Sioris, J. Skupin, S. Slijkhuis, P. Stammes, and M. Wuttke, "SCIAMACHY Level 1 data: calibration concept and in-flight calibration," Atmos. Chem. Phys. Discuss. **5**, 8925–8977 (2006).
26. U. Böttger, J. Nieke, and D. Schläpfer, "Assessing polarization effects for the airborne imaging spectrometer APEX," Adv. Radio Sci. **4**, 323–328 (2006).
27. A. Berk, L. S. Bernstein, and D. C. Robertson, "MODTRAN: a moderate resolution model for LOWTRAN7," Report GL-TR-89-0122 (Air Force Geophys. Lab, 1989), p. 38.
28. D. Schläpfer, "MODO: an interface to MODTRAN4 for the simulation of imaging spectrometry at-sensor signals," in *10th JPL Airborne Earth Science Workshop* (JPL, 2001), pp. 343–350.
29. T. Schwarzmaier, A. Baumgartner, P. Gege, C. Köhler, and K. Lenhard, "DLR's new traceable radiance standard 'RASTA'," in *IGARSS* (IEEE, 2012).
30. D. R. Taubert, J. Hollandt, P. Sperfeld, S. Pape, A. Höpe, K.-O. Hauer, P. Gege, T. Schwarzmaier, K. Lenhard, and A. Baumgartner, "Providing radiometric traceability for the calibration home base of DLR by PTB," AIP Conf. Proc. **1531**, 376–379 (2013).
31. L. Guanter, R. Richter, and J. Moreno, "Spectral calibration of hyperspectral imagery using atmospheric absorption features," Appl. Opt. **45**, 2360–2370 (2006).